FEBS Open Bio 5 (2015) 107–116

FEBS openbio

journal homepage: www.elsevier.com/locate/febsopenbio

MutT from the fish pathogen *Aliivibrio salmonicida* is a cold-active nucleotide-pool sanitization enzyme with unexpectedly high thermostability

Kjersti Lian [a], Hanna-Kirsti S. Leiros [a,*], Elin Moe [a,b,*]

[a] The Norwegian Structural Biology Center (NorStruct), Department of Chemistry, The Arctic University of Norway, 9037 Tromsø, Norway
[b] Macromolecular Crystallography Unit, Instituto de Tecnologia Química e Biológica (ITQB), Universidade Nova de Lisboa, Av. da República – EAN, 2780-157 Oeiras, Portugal

ARTICLE INFO

Article history:
Received 19 November 2014
Revised 13 January 2015
Accepted 27 January 2015

Keywords:
MutT
8-oxo-dGTP
Cold adaptation
Temperature stability
Nucleotide sanitization

ABSTRACT

Upon infection by pathogenic bacteria, production of reactive oxygen species (ROS) is part of the host organism's first line of defence. ROS damage a number of macromolecules, and in order to withstand such a harsh environment, the bacteria need to have well-functioning ROS scavenging and repair systems. Herein, MutT is an important nucleotide-pool sanitization enzyme, which degrades 8-oxo-dGTP and thus prevents it from being incorporated into DNA. In this context, we have performed a comparative biochemical and structural analysis of MutT from the fish pathogen *Aliivibrio salmonicida* (*As*MutT) and the human pathogen *Vibrio cholerae* (*Vc*MutT), in order to analyse their function as nucleotide sanitization enzymes and also determine possible cold-adapted properties of *As*MutT. The biochemical characterisation revealed that both enzymes possess activity towards the 8-oxo-dGTP substrate, and that *As*MutT has a higher catalytic efficiency than *Vc*MutT at all temperatures studied. Calculations based on the biochemical data also revealed a lower activation energy (E_a) for *As*MutT compared to *Vc*MutT, and differential scanning calorimetry experiments showed that *As*MutT displayed an unexpected higher melting temperature (T_m) value than *Vc*MutT. A comparative analysis of the crystal structure of *Vc*MutT, determined to 2.42 Å resolution, and homology models of *As*MutT indicate that three unique Gly residues in loops of *Vc*MutT, and additional long range ion-pairs in *As*MutT could explain the difference in temperature stability of the two enzymes. We conclude that *As*MutT is a stable, cold-active enzyme with high catalytic efficiency and reduced E_a, compared to the mesophilic *Vc*MutT.

1. Introduction

When microbes attack a host, phagocytes produce reactive oxygen species (ROS) as a first line of defence [1–3]. These, together with oxygen radicals generated through normal cellular metabolism or by ionising radiations, lead to oxidative stress in the bacterial cell. A common damage generated by ROS is the oxidation of guanine, resulting in the generation of 8-oxoG in DNA or 8-oxo-dGTP in the nucleotide pool, which later can be incorporated in DNA (Fig. 1) [4,5]. 8-oxoG base pairs with both adenine and cytosine in DNA, which consequently can induce A:T to C:G and G:C to T:A mutations that potentially are lethal to the organism [4,5]. Therefore, organisms possess efficient ROS scavenging and repair systems for preventing mutations [6].

The mutator enzyme MutT hydrolyses the 8-oxoG containing deoxyribose or ribonucleoside triphosphates to their corresponding monophosphates and inorganic pyrophosphate (PP_i) and thus plays an important role in the cell's sanitization system to prevent incorporation of 8-oxo-dGTP into DNA (Fig. 1) [4,5]. *In vitro* experiments have shown that 8-oxo-dGTP is the best substrate for *Escherichia coli* MutT (*Ec*MutT) with a K_m value of 0.081 μM that is 13,500 fold lower than that of dGTP (1100 μM) [7]. It was also shown that the enzyme has high affinity for the reaction product 8-oxo-dGMP with a K_D of 52 nM that is 34,600 fold lower than that

Abbreviations: 8-oxoG, 8-oxo-Guanine; Nudix, nucleoside diphosphates linked to some other moiety X; RMSD, root mean square deviation; MTH1, MutT homologue 1 from human; A:T to C:G, adenine:thymine to cytosine:guanine; NMR, nuclear magnetic resonance; DSC, differential scanning calorimetry; ROS, reactive oxygen species; E_a, activation energy

* Corresponding authors. Address: The Norwegian Structural Biology Center (NorStruct), Department of Chemistry, The Arctic University of Norway, 9037 Tromsø, Norway (H.-K.S. Leiros, E. Moe).

E-mail addresses: hanna-kirsti.leiros@uit.no (H.-K.S. Leiros), elin.moe@uit.no (E. Moe).

http://dx.doi.org/10.1016/j.fob.2015.01.006
2211-5463/

of dGMP (1.8 mM) [8]. The tight binding of the reaction product was later confirmed by determination of both the solution and X-ray crystal structures of *Ec*MutT in complex with 8-oxo-dGMP [9,10].

The MutT enzyme is widespread in nature and representatives are found in eukaryotes, prokaryotes, archaea and viruses [11]. It belongs to a superfamily of enzymes shown to require two divalent cations for activity [12,13]. Members of this family are recognised by a highly conserved 23-residue motif, or Nudix box, GX_5EX_7-REUXEEXGU, where U is a bulky hydrophobic or aliphatic residue and X is any residue [14,15]. The Nudix box forms a loop-α-helix-loop structural motif [16] that constitutes the active site.

Structures of MutT enzymes have been determined from various sources. *Ec*MutT was the first Nudix hydrolase to have its structure determined and mechanism studied in detail [9,10]. The structure of human MutT (MTH1) was solved by NMR [17], and although *Ec*MutT and MTH1 share poor sequence similarity outside the conserved Nudix motif, they adopt a similar globular and compact structure with the parallel portion of a β-sheet sandwiched between two α-helices, forming an α + β fold.

The interest in studying MutT enzymes have drastically increased based on recent findings that inhibitors of MTH1 can be used as anti-cancer drugs [18,19]. By targeting MTH1 with inhibitors the cancer cells will not be able to clean up the oxidised nucleotide pool and thus increase the cancer cell's sensitisation to cancer treatment. This finding also opens for investigation of use of MutT inhibitors for treatment of infections by pathogenic bacteria as an alternative to antibiotics.

Enzymes from cold-adapted organisms are characterised by an increased catalytic efficiency, lower temperature optimum for activity, lower temperature stability and reduced activation energy (E_a) compared to their mesophilic homologues (reviewed in [20]). It is suggested that these features originate from an increased structural flexibility [21], however the underlying molecular mechanisms for the cold-adapted properties are still not fully understood.

Here we have studied MutT from the psychrophilic fish pathogen *Aliivibrio salmonicida* (*As*MutT) and the mesophilic human pathogen *Vibrio cholerae* (*Vc*MutT) in order to obtain more information regarding their function as nucleotide sanitization enzymes and to study cold-adapted properties of *As*MutT, through enzyme kinetic measurements, differential scanning calorimetry, X-ray structure determination and homology modelling. Our findings show that *As*MutT possesses cold-adapted properties with a higher catalytic efficiency than *Vc*MutT mainly caused by higher k_{cat} values, lower K_m, and lower E_a due to lower activation enthalpy ($\Delta H^{\#}$). However *As*MutT exhibits an unexpected higher overall stability than *Vc*MutT. The comparative analysis of the crystal structure of *Vc*MutT, determined to 2.42 Å resolution, and homology models of *As*MutT shows that *Vc*MutT possesses additional Gly residues in dynamic loops and *As*MutT possesses additional long range ion-pairs which could explain the difference in stability.

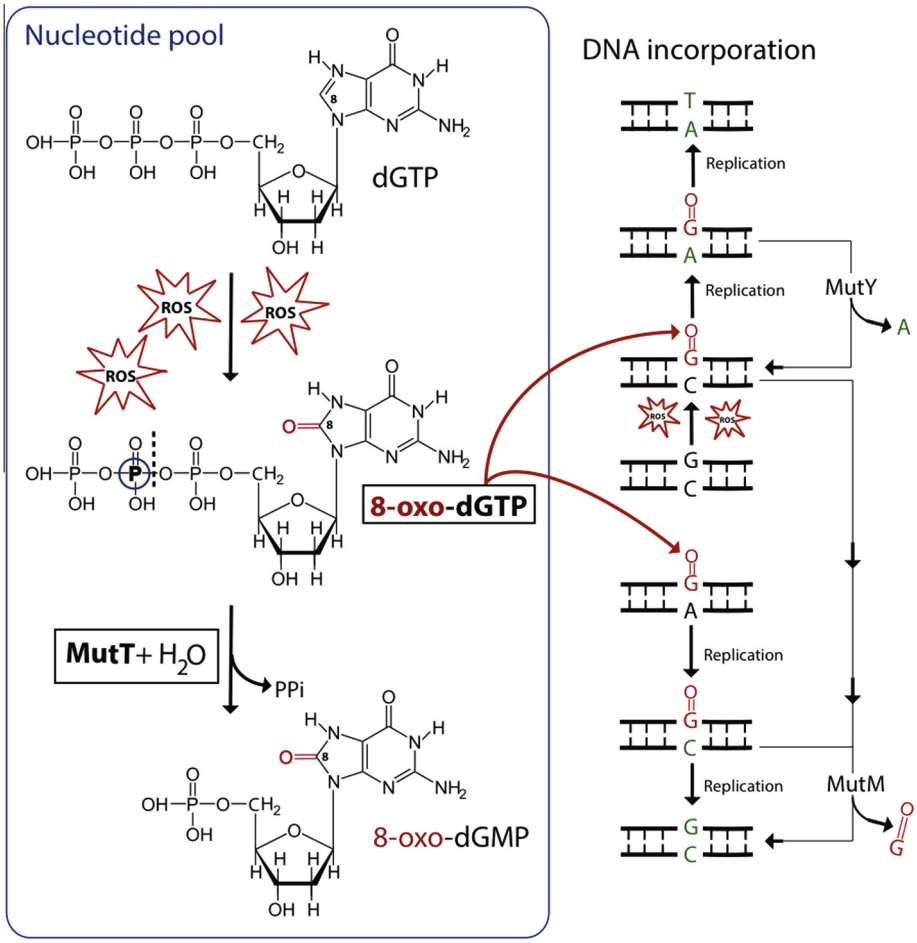

Fig. 1. A common damage generated by ROS is the oxidation of guanine, and it is formed in DNA either by direct guanine oxidation, or by incorporation of 8-oxoG from the nucleotide pool. MutT catalyses the hydrolysis of 8-oxo-GTP by nucleophilic substitution at the β phosphorus site, yielding 8-oxo-dGMP and inorganic pyrophosphate (PP_i). When 8-oxoG is incorporated in DNA against adenine or cytosine, the organism is equipped with a large mechanism system to counteract the mutagenic effects of 8-oxoG. Here, the glycosylases from base excision repair pathway MutM and MutY function to prevent T:A to G:C and G:C to T:A mutations respectively.

We conclude that both *As*MutT and *Vc*MutT are functional MutT enzymes within their respective organisms, and that *As*MutT is able to function well in its natural cold environment due to optimised substrate interactions (lower K_m) and high substrate turnover (higher k_{cat}).

2. Materials and methods

2.1. Cloning

The genes encoding *As*MutT (VSAL_I2636) and *Vc*MutT (VC_2392) were inserted into the pDest14 expression vector using Gateway technology following the manufacturer's instructions (Invitrogen), as described previously for *Deinococcus radiodurans*uracil-DNA N-glycosylase [19]. The constructs contained nucleotides encoding a 6 × His-tag immediately upstream of the gene using the following primers (Sigma–genosys): FAsMutT: 5′-CAT CAC CAT CAC CAT CAC AAG CGT GTA CAT ATT GTG-3′, RAsMutT: 5′-GGG GAC CAC TTT GTA CAA GAA AGC TGG GTC TTA TCT TAA GTA ACA TGT CAT CAC-3′, FVcMutT: 5′-CAT CAC CAT CAC CAT CAC TTG AAA CGC ATC CAC ATT GTT GCA G-3′, RVcMutT: 5′-GGG GAC CAC TTT GTA CAA GAA AGC TGG GTC TTA ACC AAA TTG AGC AAT CAC TTG C-3′, FDRHISTAG: 5′-G GGG ACA AGT TTG TAC AAA AAA GCA GGC TTC GAA GAT AGA ACC ATG CAT CAC CAT CAC CAT CAC-3′. The genes were first amplified using the primers FAs/FVcMutT and RAs/RVcMutT in order to engineer the N-terminal 6 × His-tag (underlined). The resulting gene products were thereafter amplified using the FDRHISTAG (containing the *att*B1 site and nucleotides encoding the His-tag) and the RAs/RVcMutT primers and used in a BP reaction along with the pDONR201 vector, and in a LR reaction along with the pDEST14 vector. The sequence of the clones was confirmed by DNA sequencing (ABI 377 DNA sequencer, GE Healthcare).

2.2. Expression and purification

BL21 AI competent cells (Invitrogen) transformed with the pDest14 vector containing the genes encoding *As*MutT and *Vc*MutT were grown at 37 °C in 1 L Luria–Bertani broth containing 100 μg mL^{-1} ampicillin and 0.1% glucose until the optical density at 600 nm (OD_{600}) reached 0.7. The temperature was set to 20 °C before expression was induced by 0.2% L-arabinose. The cells were harvested 16 h post-induction at 5000 rpm and resuspended in buffer A (50 mM Tris–HCl pH 7.5, 150 mM NaCl, 10 mM $MgCl_2$, and 5 mM 2-mercaptoethanol). Protease inhibitors (Roche) were added prior to cell disruption by sonication (Vibra-Cell VCX 750, IDE) and the lysate was cleared by centrifugation at 13,000 rpm for 20 min. The resulting protein extract was loaded onto a 1 mL HisTrap HP column (GE Healthcare) equilibrated with buffer A. The column was washed with 5% buffer B (Buffer A supplemented with 500 mM imidazole) to remove weakly bound proteins before the bound proteins were eluted using a 20 mL gradient to 100% buffer B. MutT containing fractions were further loaded onto a Superdex 75 10/300 GL column (GE Healthcare) using buffer A. Protein purity was determined by analysis on 4–20% SDS–PAGE (Pierce) stained with Simply Blue SafeStain (Invitrogen). The identity of the protein was confirmed using mass spectrometry (Waters® Micromass® MALDI micro MX).

2.3. Activity assay and enzyme kinetic measurements

The activity of MutT was monitored using an assay adapted from Svensson et al. [22]. By mixing 8-oxo-dGTP [10–50 μM] (Jena Bioscience), *As*MutT [64 nM] or *Vc*MutT [30 nM], enzyme buffer (250 mM Tris–HCl pH 7.5, 750 mM NaCl and 50 mM $MgCl_2$) and pyrophosphatase [0.08 U] (Sigma) in a total volume of 100 μL, we were able to detect free phosphate in solution by adding malachite green working solution containing 10 parts MG-stock prepared according to Baykov et al. [23], 2.5 parts 8% ammonium molybdate (Sigma), and 0.2 parts 11% Tween-20 solution. Here a conjugate between malachite green, molybdate and phosphate makes it possible to measure absorbance at 630 nm (OD_{630}) using Spectramax M2 (Molecular Devices). All measurements were performed in triplicate. OD_{630} values were converted to phosphate concentration for each sample using a standard curve established using various known phosphate concentrations. V_{max}, k_{cat} and K_m values were determined by fitting the data points to the Michaelis–Menten equation using non-linear regression analysis in GraphPad Prism Software (version 6.0d).

Thermodynamic activation parameters were calculated using the following equations [21]:

$$\Delta G^{\#} = RT \times (\ln k_B T/h - \ln k_{cat}) \quad (1)$$

$$\Delta H^{\#} = E_a - RT \quad (2)$$

$$\Delta S^{\#} = (\Delta H^{\#} - \Delta G^{\#})/T \quad (3)$$

where $\Delta G^{\#}$ is the free energy of activation, $\Delta H^{\#}$ is the activation enthalpy, $\Delta S^{\#}$ is the activation entropy, R is the gas constant (8.314 J mol^{-1} K^{-1}), k_B is the Boltzmann constant (1.3805×10^{-23} J K^{-1}), h the Planck constant (6.6256×10^{-34} J s) and T the temperature in kelvin.

To determine the E_a of *As*MutT and *Vc*MutT, the enzymes (*As*MutT at 64 nM and *Vc*MutT at 30 nM) were incubated with nine different substrate concentrations of 8-oxo-dGTP (Jena Bioscience) ranging from 10 to 50 μM at 4, 11, 18, 25, 32, and 37 °C in a total reaction volume of 100 μL (as described above). From these results we could calculate the E_a, by taking the natural logarithm of the Arrhenius equation (Eq. (4)) and plotting a linear regression curve ($ln\ k_{cat}$ as a function of $1/T$). The E_a value can be derived from the slope of this curve ($-E_a/R$).

$$\ln k_{cat} = \ln(A) - E_a/R(1/T) \quad (4)$$

2.4. Stability measurements by DSC

DSC experiments were executed on a Nano-Differential Scanning Calorimeter III, model CSC6300 from Calorimetry Sciences Corporation (Lindon, USA). The enzymes were prepared by dialysis over night at 4 °C in a Pierce Slide-A-Lyzer dialysis cassette from Thermo Fisher Scientific Inc (Rockford, USA) with a 10 kDa cut-off, against 1 L of dialysis buffer containing 25 mM Hepes pH 7.5, 150 mM NaCl, 10 mM $MgCl_2$, and 5 mM 2-mercaptoethanol. The enzymes were further filtered using a 0.2 μm syringe filter (Millipore, Billerica, USA), and diluted in dialysis buffer to a final enzyme concentration of 1 mg mL^{-1}. The dialysis buffer was used as reference buffer, and like the enzyme, it was degassed for approximately 15 min. before being loaded into the reference and sample DSC cells, respectively. The scans were executed between 10 and 80 °C at heating and cooling rates of 1 °C min^{-1} at a constant pressure of 3 atm. The experiments were carried out in triplicates.

2.5. Crystallization and structure determination of VcMutT

*Vc*MutT was crystallized with reservoir solution containing 0.2 M lithium sulphate, 0.1 M Tris–HCl pH 8.5, and 1.26 M ammonium sulphate by the hanging drop method, and the drops were made by mixing 1 μl 10 mg mL^{-1} protein and 1 μL reservoir solution. The quartz-shaped crystals were cryoprotected with

reservoir solution supplemented with 12.5% ethylene glycol and flash-frozen in liquid nitrogen.

X-ray data was collected at the European Synchrotron Radiation Facility (ESRF), France, on the ID14-EH1 beamline with a crystal to detector distance of 254 mm, 1.5 s exposure per frame, 0.5° oscillation, 3 passes and the final dataset included 55° of data. The images were integrated and scaled with XDS [24] and the structure factors were obtained with Truncate in the CCP4 suite [25]. The crystal belonged to space-group $P4_12_12$ or $P4_32_12$ with cell axis of $a = b = 81.15$ Å and $c = 90.57$ Å. The structure was solved by molecular replacement, using the *Vc*MutT sequence and the *Ec*MutT-Mn^{2+} bound holo form (PDB: 3A6V) as search model. There was clearly one better solution in $P4_12_12$ compared to the other possible space group. MolRep generated a homology model that was input for a second molecular replacement run in Phaser [26], and this solution was refined further with Translation/Libration/Screw (TLS) and restrained refinement REFMAC 5.5 [25]. There are two molecules in the asymmetric unit resulting in a solvent content of 51%. The model was inspected and finalised in Coot [27].

2.6. Molecular modelling of AsMutT and VcMutT

Two homology models of *As*MutT were generated by target-template alignment in Swiss-Model [28]. The first model, referred to as *As*MutT-open, was built using the crystal structure of *Vc*MutT from this work as a reference that displays 58% sequence identity with *As*MutT. The second model, referred to as *As*MutT-closed, was generated using the *Ec*MutT-8-oxo-dGMP-Mn (II) structure (PDB: 3A6U) as a template. A homology model of *Vc*MutT in a closed conformation was also generated from the same *Ec*MutT structure (PDB: 3A6U) and is denoted *Vc*MutT-closed.

2.7. Structural analysis and interaction calculations

For the structural comparison, we included the two *Vc*MutT monomers A and B, the *As*MutT-open homology model and the four *Ec*MutT crystal structures with 8-oxo-dGMP-Mn (PDB: 3A6U), 8-oxo-dGMP (PDB: 3A6T), Mn bound (PDB: 3A6V) and Apo (PDB: 3A6S).

The program HBPLUS v3.15 [29] was used to calculate hydrogen bonds satisfying the following criteria for the parameters donor (D), acceptor (A), acceptor Antecedents and (calculated) hydrogen (H): maximum distances for D–A, 3.5 Å and H–A, 2.5 Å; minimum angle for D–H–A, D–A–AA and H–A–AA of 90°.

Ion pair formation was investigated by the WHAT IF Web Interface (http://swift.cmbi.ru.nl/servers/html/index.html) [30] with interatomic distances <6 Å or <4 Å between the side chains of Asp or Glu to Arg, Lys or His residues.

3. Results and discussion

3.1. MutT from A. salmonicida and V. cholerae

The Nudix hydrolase MutT is part of the nucleotide sanitization system and is thus an important tool to protect pathogens from oxidative stress induced by heir host during bacterial infection. Here we have biochemically and structurally characterised the MutT enzymes from the fish pathogen *A. salmonicida* (*As*MutT) and human pathogen *V. cholerae* (*Vc*MutT) in order to determine their enzymatic, stability and structural properties. Primary sequence analysis of *Vc*MutT, *As*MutT and *Ec*MutT enzymes shows that *As*MutT and *Vc*MutT are highly conserved displaying 58% sequence identity and more distantly related to *Ec*MutT with sequence identities of 40.6% and 41.6% respectively (Fig. 2). When aligning the Nudix motif (residues 39–61) of these three enzymes, we see that it is highly conserved, with substitutions only in position 44, 47, and 56 where *As*MutT has Asp44, Ala47 and Asn56, compared to Gly44, Arg47 and Glu56 in *Vc*MutT.

3.2. Enzyme kinetics and activation energy calculations

In order to analyse the ability of *As*MutT and *Vc*MutT to perform hydrolysis of nucleoside- and deoxynucleoside triphosphate substrates, we performed activity assays of both enzymes with an 8-oxo-dGTP substrate in the presence of pyrophosphatase. Since we also wanted to identify potentially cold-adapted properties of *As*MutT, the assay was performed at six different temperatures for both enzymes (4, 11, 18, 25, 32 and 37 °C). The results (Table 1) show that both *As*MutT and *Vc*MutT possess activity for 8-oxo-dGTP and can thus be considered as MutT enzymes. Cold-adapted enzymes usually show a higher catalytic efficiency than their mesophilic homologues [20,21,31], and the results here show that *As*MutT indeed possesses significantly higher k_{cat}/K_m values compared to *Vc*MutT at all temperatures studied. The higher catalytic efficiency for *As*MutT is mainly caused by high k_{cat} values, but also slightly lower K_m values at 18, 25, 32 and 37 °C. We also observed that *Vc*MutT is not active at 4 °C whereas *As*MutT is highly active at this temperature, clearly indicating that *As*MutT is adapted for function at its naturally low temperature environment, while *Vc*MutT works better at its naturally higher temperature environments. Note that the k_{cat} values are similar for both enzymes at their respective optimum growth temperatures, 12 °C for *A. salmonicida* and 37 °C for *V. cholerae*.

Cold-adapted enzymes are usually characterised by lower E_a than their mesophilic homologues in an enzymatic reaction [21,32]. E_a of *As*MutT and *Vc*MutT was derived from the slope ($-E_a/R$) of the Arrhenius plot ($ln\ k_{cat}$ as a function of 1/T) made from measurements of k_{cat} at six different temperatures (Fig. 3A). The results show that *As*MutT has an E_a of 36.26 kJ mol^{-1} compared to 45.67 kJ mol^{-1} for *Vc*MutT, which allows *As*MutT to perform catalysis more efficiently at low temperatures. The calculations of the $\Delta H^{\#}$ and $\Delta S^{\#}$ of activation revealed lower values for *As*MutT (Table 1), as is typically observed for psychrophilic enzymes [33].

3.3. Thermal stability of AsMutT and VcMutT

In order to compare the overall thermal stability of *As*MutT and *Vc*MutT, DSC experiments were performed. The results (Table 1 and Fig. 3B) show that *Vc*MutT possesses a slightly lower overall stability, with a melting temperature (T_m) of 54.70 ± 0.22 °C compared to *As*MutT, which has a T_m of 57.80 ± 0.09 °C. The thermal denaturation of both *As*MutT and *Vc*MutT enzymes was irreversible and aggregation was evident in the samples extracted from the calorimeter cells. Therefore, attempts to calculate more thermodynamic data were prevented.

3.4. The crystal structure of VcMutT

The crystal structure of *Vc*MutT was determined to 2.42 Å resolution (Table 2; PDB: 4V14) by molecular replacement. Different *Ec*MutT models were tested, and the open Mn bound form (PDB: 3A6V) gave higher rotational and translation scores and was thus used as the molecular replacement model. *Vc*MutT adopts an α-β-α sandwich structure with seven β-strands (β1-7) and two α-helices (α1-2) as shown in Fig. 4A. This fold is similar to *Ec*MutT and is conserved in the Nudix hydrolase family of proteins. In *Vc*MutT, the Nudix motif (*i.e.* the MutT signature) starts with Gly39 and makes a strand-loop-helix-loop (SLHL) motif (β4-loop-α1-loop), terminating with Ile61. *Vc*MutT was crystallized with two protein molecules (A and B) in the asymmetric unit, with average B-factors of 48.9 and 63.8 $Å^2$ respectively (Table 2). The root

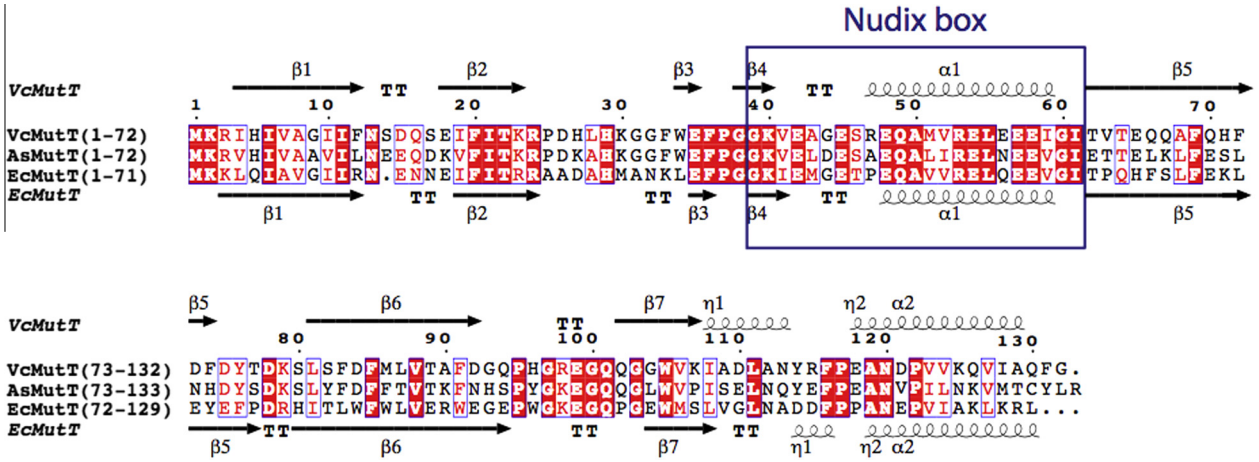

Fig. 2. Sequence alignment of *Vc*MutT, *As*MutT and *Ec*MutT with the secondary structure elements of *Vc*MutT (top) and *Ec*MutT (bottom, PDB: 3A6S). Nudix box residues 39–61 ($GX_5EX_7REUXEEXGU$, where U is a bulky hydrophobic residue and X is any residue).

Table 1
Kinetic constants at 4–37 °C, and thermodynamic activation energy parameters calculated (kJ mol^{-1}) for the psychrophilic *As*MutT and the mesophilic *Vc*MutT.

Enzyme	E_a	T	K_m	k_{cat}	k_{cat}/K_m	$\Delta G^{\#}$	$\Delta H^{\#}$	$T\Delta S^{\#}$
	(kJ mol^{-1})	(°C)	(μM)	(s^{-1})	(s^{-1} μM^{-1})	(kJ mol^{-1})		
*As*MutT	36.26 ± 0.14	4	1.78 ± 1.21	0.534 ± 0.029	0.30 ± 0.12	69.15	33.96	−35.20
		11	2.93 ± 1.42	0.713 ± 0.039	0.24 ± 0.03	70.28	33.90	−36.38
		18	3.21 ± 0.99	0.974 ± 0.039	0.303 ± 0.04	71.31	33.84	−37.47
		25	10.74 ± 1.80	1.54 ± 0.08	0.144 ± 0.045	74.09	33.78	−40.31
		32	14.97 ± 2.29	2.04 ± 0.11	0.114 ± 0.049	72.98	33.72	−39.26
		37	18.17 ± 0.90	2.83 ± 0.25	0.134 ± 0.057	73.38	33.68	−39.70
*Vc*MutT[a]	45.67 ± 0.11	4	n/a	n/a	n/a	n/a	n/a	n/a
		11	1.99 ± 0.68	0.153 ± 0.004	0.077 ± 0.006	73.92	43.31	−30.61
		18	5.59 ± 0.71	0.252 ± 0.006	0.045 ± 0.008	74.59	43.25	−31.34
		25	12.84 ± 0.65	0.491 ± 0.008	0.038 ± 0.012	74.78	43.19	−31.59
		32	17.24 ± 2.54	0.573 ± 0.032	0.033 ± 0.013	76.21	43.13	−33.08
		37	25.65 ± 5.49	0.77 ± 0.074	0.030 ± 0.014	76.73	43.09	−33.64

[a] n/a indicates no activity detected.

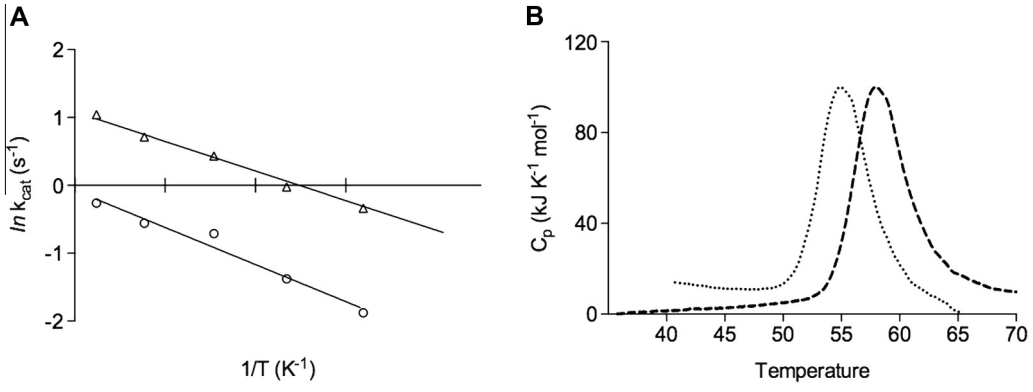

Fig. 3. (A) Arrhenius plot of the enzyme activity of *Vc*MutT (open circles), and *As*MutT (open triangles) using Eq. (4). The activation energies (E_a) were found to be 45.67 ± 0.11 kJ mol^{-1} (*Vc*MutT) and 36.26 ± 0.14 kJ mol^{-1} (*As*MutT). (B) Thermal stability measurements of mesophilic *Vc*MutT (. . .) and psychrophilic *As*MutT (—) revealed melting temperatures (T_m) of 54.70 ± 0.22 °C (*Vc*MutT) and 57.80 ± 0.09 °C (*As*MutT). The experiments were monitored by DSC at a scan rate of 1 °C min^{-1}, and the thermograms were base line subtracted and normalised towards the protein concentrations.

mean square deviation (RMSD) between molecules A and B is 0.48 Å^2 for the Cα atoms, and for simplicity only molecule A, with the lowest mean B-factor, will be referred to hereafter. There are some regions with poor electron density, hence the residues were left out of the final model (A1, A28-29, A76-A79, A132, B24-32, B77-79 and B132).

For Chain A of *Vc*MutT compared to *Ec*MutT the RMSD and no of aligned Cα atoms are: 1.72 Å for 119 Cα atoms compared

Table 2
Statistics from the X-ray data collection and refinement of *Vc*MutT. The numbers in parentheses represent values in the highest of 10 resolution shells, and the resolution limits for these are indicated.

X-ray statistics	*Vc*MutT
PDB entry	4V14
Beamline	ESRF, ID14-EH1
Space group	$P4_12_12$
Unit cell (Å)	$a = b = 81.15$, $c = 90.57$
Resolution (Å)	50–2.42 Å
(highest bin)	(2.55–2.42)
Wavelength (Å)	0.934
No. of unique reflections	11 909
Multiplicity	4.4 (4.4)
Completeness (%)	99.1 (100)
Mean ($<I>/<\sigma_I>$)	21.1 (2.8)
R_{merge} (%) [a]	5.2 (59.6)
Wilson B-factor (Å^2)	55.69
Refinement	
Resolution (Å)	10–2.42
R-factor (all reflections) (%)[b]	23.02
R-free (%)[b]	30.21
No. of protein atoms	1982
No. of water molecules	48
RMDS bond lengths (Å)	0.019
RMSD bond angles (°)	1.75
Average B-factor (Å^2)	
All atoms	56.2
Chain A/B	48.9/63.8
Water molecules	55.1

[a] $R_{merge} = (\sum_h \sum_i |I_i(h) - <I(h)>|)/(\sum_h \sum_I I(h))$, where $I_i(h)$ is the ith measurement of reflection h and $<I(h)>$ is the weighted mean of all measurements of h.
[b] $\sum_h ||F_{obs}| - |F_{calc}|| / \sum_h |F_{obs}|$, where $|F_{obs}|$ and $|F_{calc}|$ are observed and calculated structure factor amplitudes for all reflections (R-factor) and the reflections applied in the test R-free set (reflections not used in the structure refinement), respectively.

*Ec*MutT-8-oxo-dGMP-Mn (PDB: 3A6U), 1.73 Å for 120 Cα atoms to *Ec*MutT-8-oxo-dGMP (PDB: 3A6T), 1.33 Å for 115 Cα atoms compared to open *Ec*MutT-Mn (Chain A, PDB: 3A6V), and 1.58 Å for 116 Cα atoms relative to *Ec*MutT-Apo (Chain A, PDB: 3A6S).

3.5. Active site comparison of AsMutT, VcMutT and EcMutT

Several residues in the loops between β2–β3 and β5–β6 (28–29 and 76–79) of *Vc*MutT were not visible in the observed electron density, indicating that these loops are flexible. For the open *Ec*MutT structure bound to Mn, residues in the first loop are also missing, but upon substrate binding the enzyme adopts a more closed conformation, in which these loops fold over the active site interacting with each other and become well defined in the *Ec*MutT complex structures (PDB: 3A6T, 3A6U). This ligand-induced conformational change is modelled in the *Vc*MutT-closed and *As*MutT-closed homology models based on *Ec*MutT-8-oxo-dGMP-Mn (PDB: 3A6U) (Fig. 4B and C).

MutT belongs to a superfamily of enzymes requiring two divalent cations for activity [12,13], and it has been shown that MutT possesses higher activity when the magnesium concentration is increased up to 10 mM [34]. Although *Vc*MutT was purified with 10 mM $MgCl_2$, no electron density could be seen in the *Vc*MutT structure corresponding to Mg^{2+}. This is not a surprise knowing that the affinity of MutT to Mg^{2+} is very low (1/50 compared to Mn^{2+}) [12]. However, when we model Mn^{2+} in *Vc*MutT-closed and *As*MutT-closed assuming it is bound in the same sites as Mn in *Ec*MutT, we observe that residues Glu54, Glu58, and the main-chain oxygen of Gly38 are potential metal binding residues compared to *Ec*MutT (PDB: 3A6U) [10,35] thus we believe Mg^{2+} can bind to our enzymes and thus contribute to the catalytic process (Fig. 4C). A second metal binding site could involve Glu54 and Glu58 in addition to water mediated interactions in both *As*MutT and *Vc*MutT, as shown for the open *Ec*MutT with Mn (PDB: 3A6V) [10].

A central question in the field is how MutT enzymes favour the recognition of 8-oxo-dGTP over dGTP? Structural studies have demonstrated that MutT undergoes conformational changes upon substrate binding [8–10]. The analyses have suggested that Asn119 (Asn120 in *As*MutT and *Vc*MutT) is especially important for the affinity between *Ec*MutT and 8-oxo-dGMP. Saraswat et al. (2004) [35] described this by performing an N119A-mutation, which led to a 1650-fold decrease in the affinity of the enzyme for 8-oxo-dGMP. The substrate-binding pocket is very well conserved when comparing *As*MutT, *Vc*MutT and also *Ec*MutT, and the Asn120 is conserved, thus also discriminating the substrate binding in *Vibrio* MutTs (Fig. 4D). A close inspection of the substrate-binding pocket also shows that both *As*MutT and *Vc*MutT possess a tyrosine residue (Tyr76), which is in a position to hydrogen bond with the oxygen atom (O8) at C8 of 8-oxo-dGTP (Fig. 4D). This feature is not present in *Ec*MutT, since it has a Phe in the same position, but Tyr76 may assist the *As*MutT and *Vc*MutT in their substrate discrimination. Additional interactions from *As*MutT or *Vc*MutT to 8-oxo-dGTP are identical and include: Arg24, His29, Phe36, Gly38, Lys40 and Lys79 (Fig. 4C and D). The phosphate group of 8-oxoG interacts with the guanidinium group of Arg24, through a metal mediated interaction with Gly38 O, and through waters to Lys79 NZ and Lys40 N atoms. The main chain atoms of Phe36 make three different hydrogen bonds to N2, N1 and O6. From the O3' atom of the deoxyribose there is a direct bond to His29 (ND1) and a water-mediated interaction to Lys79 NZ.

3.6. Structural explanations for cold-active properties

Our enzymatic assays have shown that *As*MutT displays cold-adapted properties with a high catalytic efficiency and a low E_a compared to its mesophilic homologue *Vc*MutT. However, the thermal stability of *As*MutT is unexpectedly higher compared to *Vc*MutT. Here we will compare the crystal structures of *Vc*MutT and *Ec*MutT, and the homology models to find structural explanations for the observed biochemical differences.

Many psychrophilic enzymes possess higher K_m values than their mesophilic counterparts, a phenomenon that has been explained by a more dynamic or flexible active site that binds its substrate weakly [33]. A low K_m value, as found for *As*MutT, indicates that it possesses a higher affinity for its substrate, which is unusual but has been observed for other cold-adapted DNA repair enzymes like uracil DNA N-glycosylase from Atlantic cod (cUNG) [36] and *A. salmonicida* [37] and for the anionic salmon trypsin (AST) [38]. Herein, the negatively charged DNA substrate binds very strongly to a positively charged active site of cUDG, and in the case of trypsin, the negative surface charge of AST was proposed to explain the tight binding of the positively charged substrate [38,39]. Upon substrate binding the surface is important and the calculated electrostatic surface potential of modelled *Vc*MutT-closed and *As*MutT-closed bound to 8-oxo-dGMP (Fig. 4E and F) illustrate this. The overall charges are not so different since *As*MutT has a net charge of −7 and *Vc*MutT −8 (Table 3), but the charge distribution is slightly altered. Here Lys27 is unique to *As*MutT (His27 in *Vc*MutT) and situated on the tip of the loop between β2 and β3, which changes conformation upon substrate binding [10], and moves closer to the substrate binding site in the closed models. Also, in the Nudix motif, Asn56 in *As*MutT is substituted by a negatively charged Glu56 in *Vc*MutT. Taken together, we believe that the presence of Lys27 in *As*MutT and Glu56 in *Vc*MutT can explain the slightly higher substrate affinity of *As*MutT for the negatively charged triphosphate tail of the substrate.

The E_a calculation of *As*MutT and *Vc*MutT enzymes was made based on the k_{cat} values of the two enzymes, and shows that

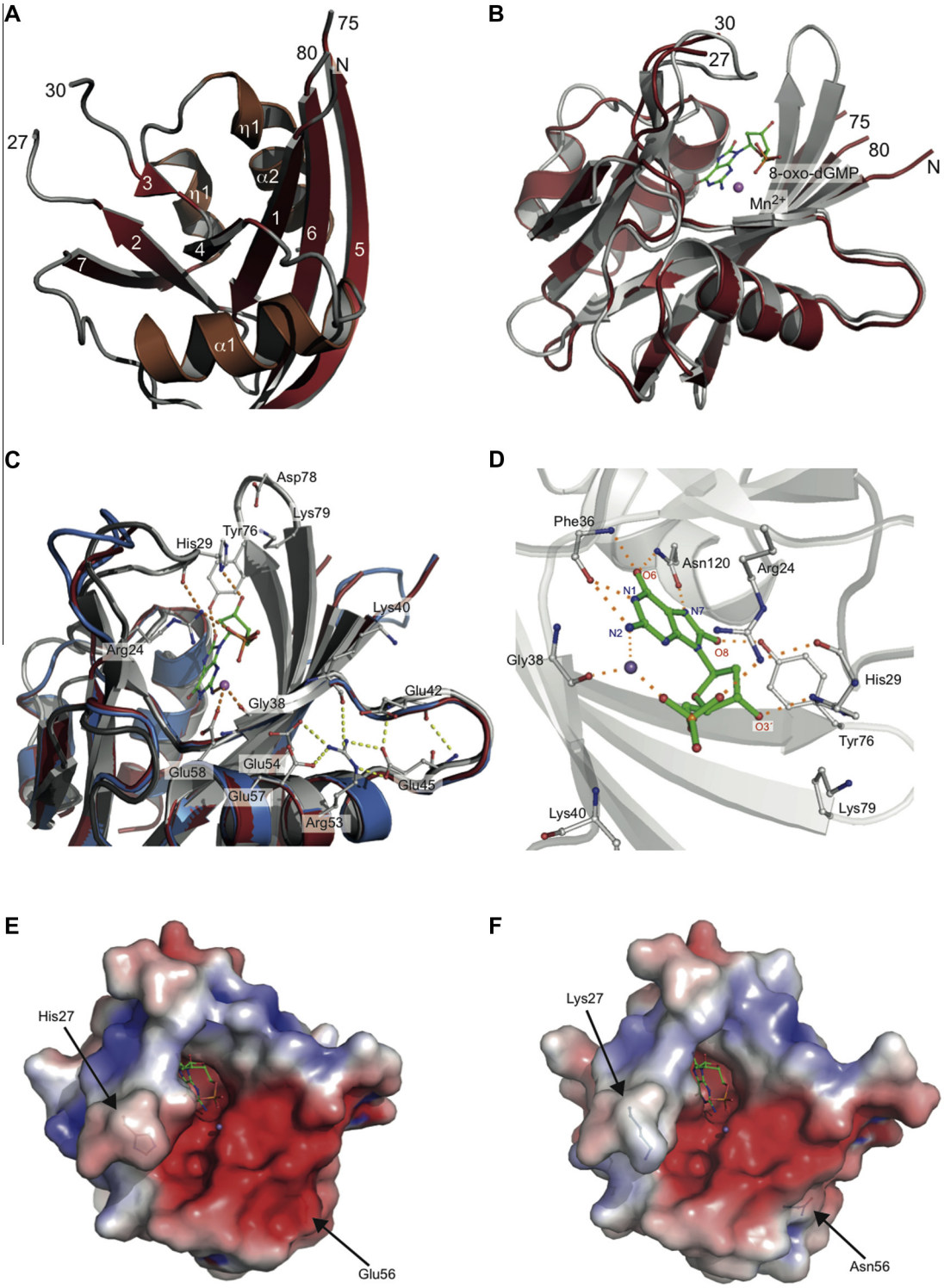

Fig. 4. (A) Ribbon diagram of the *Vc*MutT X-ray structure with β-strands in firebrick red, α-helices in brown and loops in grey. (B) Homology model of *Vc*MutT-closed (grey) made from *Ec*MutT-8-oxo-dGTP-Mn superimposed on *Vc*MutT (firebrick red). 8-oxo-dGMP and Mn^{2+} are modelled from the *Ec*MutT-8-oxo-dGTP-Mn structure. (C) Hydrogen bonding interactions between 8-oxo-dGMP and *Vc*MutT (crystal structure in firebrick red and closed homology model in grey). The super imposed *As*MutT models (closed in dark-grey and open in sky-blue) are also shown. Residues involved in Mn^{2+} coordination and residues promoting conformational stabilization to the enzymes structure are indicated. (D) Hydrogen bonds between the *Vc*MutT-closed model and 8-oxo-dGMP. Electrostatic surface of the homology model of (E) *Vc*MutT-closed and (F) *As*MutT-closed with important residue differences highlighted. (For interpretation of the references to colour in this figure legend, the reader is referred to the web version of this article.)

*As*MutT possesses a lower E_a compared to *Vc*MutT, and thus agrees with previous findings for other cold-adapted enzymes (reviewed in Feller et al. 2013) [40]). The main explanation for the reduced E_a lies in the $\Delta H^{\#}$ of the enzyme, which indicates that a reduced number of enthalpy related interactions have to be broken during transition-state formation [41] and that the k_{cat} is thus less dependent on temperature. In order to find an explanation for our observed difference in $\Delta H^{\#}$, we inspected the *As*MutT-closed and *Vc*MutT-closed models and analysed the protein-substrate interactions (Fig. 4C). The results show that all of the interactions between

Table 3
Sequence and structural characterisation of *As*MutT (homology model), *Vc*MutT and four *Ec*MutT structures (PDB: 3A6U, 3A6S, 3A6T, 3A6V). Theoretical pI for *As*MutT and *Vc*MutT was calculated from the full-length sequences including the 6× His-tag. Residues included in the various class definitions are net charged, polar, hydrophobic, and aromatic residues.

	*As*MutT	*Vc*MutT		*Ec*MutT			
Chain, ligand		A	B	8-oxo-dGMP-Mn	8-oxo-dGMP	Mn	Apo
PDB ID	Model	4V14		3A6U	3A6T	3A6V	3A6S
T_m (°C)	57.80	54.70		–			
No. amino acids per monomer in PDB (in gene construct)	129 (135)	124 (134)	119	126 (129)	127	122	125
Calculated pI[a]	5.77 (5.10)	5.71 (5.01)		5.01			
Net charge[b]	−7	−8		−7			
Polar residues[c] (%)	27.3	27.4		21.9			
Hydrophobic residues[d] (%)	38.7	39.7		47.3			
Aromatic residues[e] (%)	11.5	11.5		10.1			
No. of Met. residues	2	3		4			
No. of Gly. residues	8	13		10			
No. of Pro. residues	6	5		9			
Arg/(Arg + Lys)	0.27	0.46		0.41			
(Leu + Ile)/(Leu + Ile + Val)	0.66	0.63		0.74			
Resolution	Model	2.42 Å	2.42 Å	2.56 Å	1.96 Å	2.00 Å	1.80 Å
No. of hydrogen bonds per residue in PDB file	0.77	0.80	0.73	0.83	0.83	0.77	0.80
No. SS[f] hydrogen bonds per residue	0.11	0.08	0.08	0.12	0.10	0.07	0.09
No. SM[g] hydrogen bonds per residue	0.12	0.12	0.08	0.17	0.16	0.14	0.14
No. MM[h] hydrogen bonds per residue	0.53	0.60	0.56	0.54	0.57	0.57	0.57
No. ion pairs <4/<6 Å	8/12	7/9	6/8	10/12	10/13	7/15	9/17
No. 2 member networks <4.0 Å	5	2	3	2	2	4	1
No. 3 member networks <4.0 Å	0	1	0	2	2	0	3
No. 4 member networks <4.0 Å	1	1	1	0	0	1	1
No. 5 member networks <4.0 Å	0	0	0	1	1	0	0

[a] Calculated pI includes 6× His-tag for *As*MutT and *Vc*MutT. (Calculated pI without 6× His-tag).
[b] Calculated with residues R, K, D and E.
[c] Polar residues G, S, T, Y, N, Q and C.
[d] Hydrophobic residues A, V, L, I, W, F, P and M.
[e] Aromatic residues F, W and Y.
[f] SS, side-chain to side-chain hydrogen bonds.
[g] SM, side-chain to main-chain hydrogen bonds.
[h] MM, main-chain to main-chain hydrogen bonds.

residues in the substrate binding pocket and the substrate are the same in *As*MutT and *Vc*MutT (Fig. 4C and D). This thus suggests that other parts of the enzyme most likely account for the observed enthalpy difference. Recently it was suggested that differences in enzyme–water interaction could explain reduced $\Delta H^{\#}$ for the cold-adapted AST compared to its mesophilic homologue Bovine trypsin [42]. An analysis of residues on the surface of *As*MutT and *Vc*MutT shows that there are many substitutions, which may change the protein–water interactions. We see in particular that *As*MutT has more charged residues on its surface, where *Vc*MutT has polar residues, *e.g.* for the surface residues 14, 17, 44, 62, 67, 70, 90, 126 (Fig. 2). This can result in reduced H-bonding network on the surface since the latter may prefer to interact with bulk solvent [42].

The higher negative value of $\Delta S^{\#}$ for *As*MutT corresponds well to previous findings of other cold-adapted enzymes and suggests that the ground state enzyme-substrate complex has a greater degree of disorder than for *Vc*MutT (reviewed in Feller et al. 2013) [40]. But a more disordered *As*MutT does not relate to the observed higher thermal stability of the enzyme. The lower $\Delta S^{\#}$ of *As*MutT is thus not rationalised in our current structure or models.

3.7. Structural elements promoting overall stability

Characterisation of the thermal stability by DSC showed that *As*MutT possesses a T_m of 57.80 °C, which is 3.10 degrees higher than for *Vc*MutT. It is unusual that cold-adapted enzymes have an increased overall stability compared to their mesophilic homologues, however it has previously been observed for some enzymes, *e.g.* isocitrate dehydrogenase from *Desulfotalea psychrophila* [43]. In order to identify specific structural determinants, which may explain the difference in temperature stability between *As*MutT and *Vc*MutT, and the unexpected high stability of *As*MutT, we compared the amino acid compositions, the content of aromatic residues, ion pairs and hydrogen bonds of the two enzymes (Table 3), and compared these values to the mesophilic *Ec*MutT. This analysis revealed that *As*MutT possesses less glycine residues compared to *Vc*MutT and *Ec*MutT (8/13/10 Gly in *As*/*Vc*/*Ec*MutT). The additional glycine residues in *Vc*MutT are found within the β-strands β1 (Gly9) and β7 (Gly104), but the ones on the surface, which is Gly44 (in the loop between β4 and α1), Gly93 (between β6 and β7) and the disordered Gly132 in the C-terminal, are all likely to contribute to the reduced thermal stability of *Vc*MutT (Fig. 5A). The (Leu + Ile)/(Leu + Ile + Val) ratio, where a high number reflect a higher thermal stability [44] is similar in all enzymes, but the Arg/(Arg + Lys) ratio is lowest in *As*MutT (Table 3) indicating lower thermal stability. However, we also found fewer flexible methionine residues in *As*MutT (2/3/4 Met in *As*/*Vc*/*Ec*MutT) and one extra proline (Pro107) in *As*MutT compared to *VcMutT* (6/5/9 Pro in *As*/*Vc*/*Ec*MutT) both promoting higher stability of *As*MutT.

Aromatic interactions are important contributors to protein stability, and *As*MutT and *Vc*MutT have 12 identical aromatic residues located in the same positions in the sequences (Fig. 2) and both have an aromatic residue in position 131 (*As*MutT Tyr131; *Vc*MutT Phe131). In addition, *As*MutT includes Tyr82, Phe86 and Tyr96, and *Vc*MutT has Phe12, Phe72 and Phe74 (Fig. 5B). For the latter, Phe72 and Phe74 form stacking interactions with each other with a distance of 4.8 Å from the two aromatic rings, that are adjacent to both Phe83 and Phe85 which again are adjacent to Phe36 and Phe116. This makes a bigger aromatic cluster in *Vc*MutT than in *As*MutT and favours overall stability of the former. The unique *As*MutT aromatic residues are all found at the surface, altering the protein water interactions. In total, the aromatic interactions

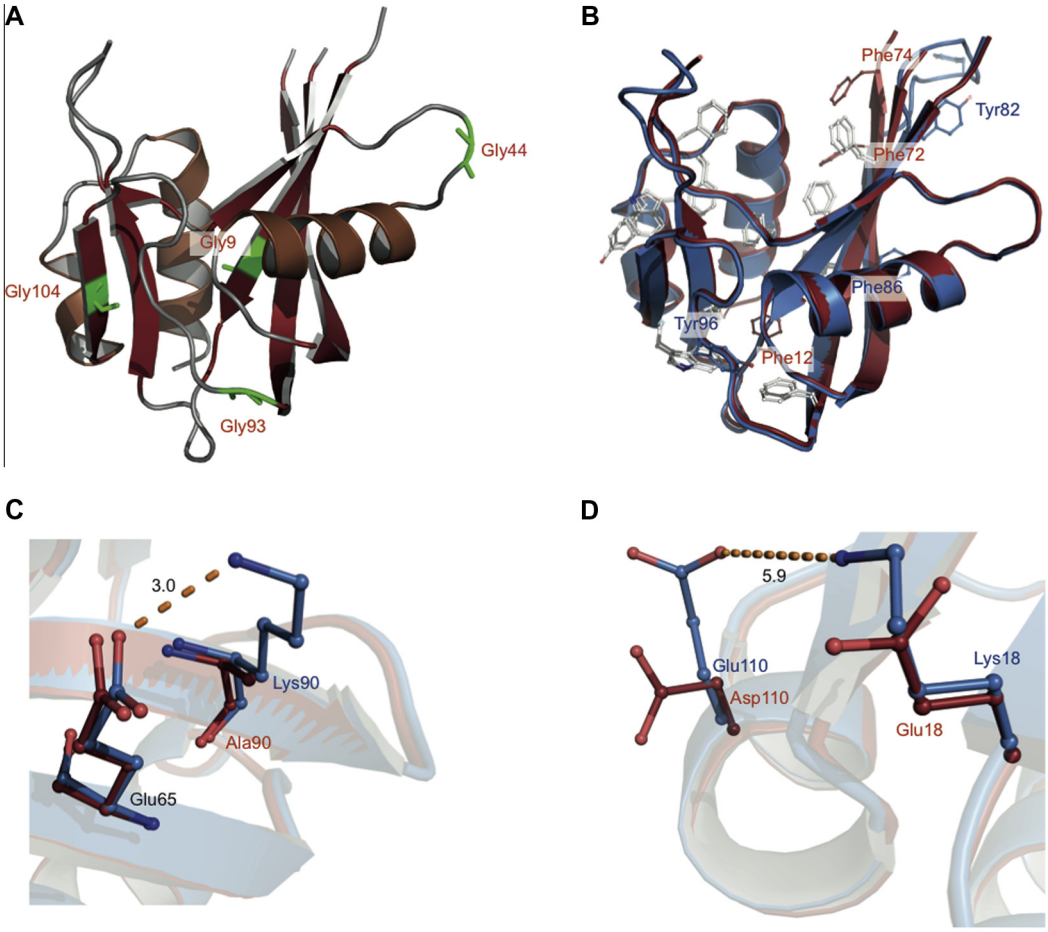

Fig. 5. (A) Ribbon diagram of *Vc*MutT with unique glycines (green) believed to contribute to reduced thermal stability. (B) Superimposition of X-ray structure of *Vc*MutT (firebrick red) and the *As*MutT-open homology model (sky-blue) with conserved aromatic residues in white. Unique aromatic residues are shown in firebrick red (*Vc*MutT) and sky-blue (*As*MutT). (C) Amino acids involved in ionic interactions in *As*MutT-open (sky-blue) which include Lys90-Glu65 and (D) Lys18-Glu110, with the corresponding *Vc*MutT residues (firebrick red). (For interpretation of the references to colour in this figure legend, the reader is referred to the web version of this article.)

favour thermal stability in *Vc*MutT due to a bigger aromatic cluster than in *As*MutT.

An analysis of ion pairs showed that there are some unique long ionic interactions in *As*MutT-open, including Lys18-Glu110 and Lys90-Glu65 (Fig. 5C and D), which gives a total of 8/12 ion pairs (<4/<6 Å) in *As*MutT-open compared to 7/9 pairs in *Vc*MutT (Table 3). In *Ec*MutT, there are more ion pairs (<4 Å) in the closed forms (PDB: 3A6U, 3A6T) than in the open apo form (PDB: 3A6S), but not the open Mn^{2+} bound structure (PDB: 3A6V). In all *Ec*MutT structures, there is one large ion pair cluster with 4 or 5 members (Table 3). The same ion pair cluster is found in both *As*MutT and *Vc*MutT with Glu42, Arg53, Glu54 and Glu54 as shown in Fig. 4C, but since the residues are conserved in both *As*MutT and *Vc*MutT they do not explain the difference in T_m. Ionic interactions and increased formation of large ionic networks at the protein surface increases the thermal stability [43] and for *As*MutT-open the two unique interactions could enhance the thermal stability. The number of H-bonds per residues in *As*MutT-open, *Vc*MutT and *Ec*MutT show comparable numbers from 0.73 to 0.83 (Table 3) and thus seem similar in the compared structures.

MutT is a small and compact monomeric enzyme (15 kDa), which is well conserved throughout evolution and has been referred to as a "house-cleaning" enzyme [45]. The unexpected high thermostability of *As*MutT does not seem to affect the catalytic efficiency of the enzyme at low temperatures, and there is no tradeoff for the enzyme function in its natural low temperature environment. Thus, we explain the high temperature stability of *As*MutT with its high conservation in nature, small and compact structure and the need of having a functional MutT enzyme available at all times in order to maintain the *A. salmonicida* genome during ROS attacks from the hosts they are invading.

4. Concluding remarks

Here we have studied MutT enzymes from the psychrophilic fish pathogen *A. salmonicida* and the mesophilic human pathogen *V. cholerae*. Our results show that both enzymes are functional MutT enzymes, catalysing the degradation of 8-oxo-dGTP to 8-oxo-dGMP and PP_i, thus both organisms have these important nucleotide sanitizing enzymes to fight ROS attacks from their host during infection. We have also shown that *As*MutT is a cold-active enzyme with higher catalytic efficiency and lower energy of activation compared to *Vc*MutT. The high efficiency is mainly caused by a high k_{cat}, which is allowed by a low $\Delta H^{\#}$ caused by a reduced number of enthalpy related interactions, which have to be broken during transition-state formation. *As*MutT showed unexpected high temperature stability, which through comparative analysis of the crystal structure of *Vc*MutT and homology models of *As*MutT, is explained by the absence of three Gly residues in loops (Gly44, Gly93, Gly132), one extra proline (Pro107) and two additional long-range ion-pairs on the enzyme surface.

Recent studies on human MutT (MTH1) have shown that there is potential for using MTH1 inhibitors as anticancer drugs [18,19]. Upon addition of MTH1 inhibitors to cancer cells, the cells were

directed to apoptosis and died. Based on this finding and the current knowledge that exists regarding bacterial MutT and their importance for the bacterial resistance to ROS upon infection, we propose that there is a potential for using MutT inhibitors in treatment of bacterial infections both in humans and animals as an alternative to antibiotics.

Acknowledgements

Provision of beam time at the European Synchrotron Radiation Source ESRF beam line ID14-EH1 is gratefully acknowledged. We are also very thankful for Joanna Timmins help to improve the manuscript. This work was supported by the FRIBIO and National Functional Genomics Program (FUGE) programme in the Research Council of Norway. EM conceived and designed the project; HKSL determined the crystal structure of *Vc*MutT and performed structure related analysis and KL cloned, expressed, purified, crystallised and characterised the enzymes. All authors were strongly involved in the data interpretation and writing of the manuscript.

References

[1] Fang, F.C. (2011) Antimicrobial actions of reactive oxygen species. mBio 2 (5), e00141.
[2] Babior, B.M. (1978) Oxygen-dependent microbial killing by phagocytes (second of two parts). N. Engl. J. Med. 298, 721–725.
[3] Babior, B.M. (1978) Oxygen-dependent microbial killing by phagocytes (first of two parts). N. Engl. J. Med. 298, 659–668.
[4] Maki, H. (2002) Origins of spontaneous mutations: specificity and directionality of base-substitution, frameshift, and sequence-substitution mutageneses. Annu. Rev. Genet. 36, 279–303.
[5] Miller, H., Prasad, R., Wilson, S.H., Johnson, F. and Grollman, A.P. (2000) 8-oxodGTP incorporation by DNA polymerase beta is modified by active-site residue Asn279. Biochemistry 39, 1029–1033.
[6] Michaels, M.L. and Miller, J.H. (1992) The GO system protects organisms from the mutagenic effect of the spontaneous lesion 8-hydroxyguanine (7,8-dihydro-8-oxoguanine). J. Bacteriol. 174, 6321–6325.
[7] Ito, R., Hayakawa, H., Sekiguchi, M. and Ishibashi, T. (2005) Multiple enzyme activities of *Escherichia coli* MutT protein for sanitization of DNA and RNA precursor pools. Biochemistry 44, 6670–6674.
[8] Saraswat, V., Massiah, M.A., Lopez, G., Amzel, L.M. and Mildvan, A.S. (2002) Interactions of the products, 8-oxo-dGMP, dGMP, and pyrophosphate with the MutT nucleoside triphosphate pyrophosphohydrolase. Biochemistry 41, 15566–15577.
[9] Massiah, M.A., Saraswat, V., Azurmendi, H.F. and Mildvan, A.S. (2003) Solution structure and NH exchange studies of the MutT pyrophosphohydrolase complexed with Mg(2+) and 8-oxo-dGMP, a tightly bound product. Biochemistry 42, 10140–10154.
[10] Nakamura, T., Meshitsuka, S., Kitagawa, S., Abe, N., Yamada, J., Ishino, T., Nakano, H., Tsuzuki, T., Doi, T., Kobayashi, Y., Fujii, S., Sekiguchi, M. and Yamagata, Y. (2010) Structural and dynamic features of the MutT protein in the recognition of nucleotides with the mutagenic 8-oxoguanine base. J. Biol. Chem. 285, 444–452.
[11] Xu, W., Jones, C.R., Dunn, C.A. and Bessman, M.J. (2004) Gene ytkD of *Bacillus subtilis* encodes an atypical nucleoside triphosphatase member of the Nudix hydrolase superfamily. J. Bacteriol. 186, 8380–8384.
[12] Frick, D.N., Weber, D.J., Gillespie, J.R., Bessman, M.J. and Mildvan, A.S. (1994) Dual divalent cation requirement of the MutT dGTPase. Kinetic and magnetic resonance studies of the metal and substrate complexes. J. Biol. Chem. 269, 1794–1803.
[13] Bhatnagar, S.K., Bullions, L.C. and Bessman, M.J. (1991) Characterization of the mutT nucleoside triphosphatase of *Escherichia coli*. J. Biol. Chem. 266, 9050–9054.
[14] Mildvan, A.S., Weber, D.J. and Abeygunawardana, C. (1999) Solution structure and mechanism of the MutT pyrophosphohydrolase. Adv. Enzymol. Relat. Areas Mol. Biol. 73, 183–207.
[15] Bessman, M.J., Frick, D.N. and O'Handley, S.F. (1996) The MutT proteins or "Nudix" hydrolases, a family of versatile, widely distributed, "housecleaning" enzymes. J. Biol. Chem. 271, 25059–25062.
[16] Koonin, E.V. (1993) A common set of conserved motifs in a vast variety of putative nucleic acid-dependent ATPases including MCM proteins involved in the initiation of eukaryotic DNA replication. Nucleic Acids Res. 21, 2541–2547.
[17] Mishima, M., Sakai, Y., Itoh, N., Kamiya, H., Furuichi, M., Takahashi, M., Yamagata, Y., Iwai, S., Nakabeppu, Y. and Shirakawa, M. (2004) Structure of human MTH1, a Nudix family hydrolase that selectively degrades oxidized purine nucleoside triphosphates. J. Biol. Chem. 279, 33806–33815.
[18] Gad, H., Koolmeister, T., Jemth, A.S., Eshtad, S., Jacques, S.A., Strom, C.E., Svensson, L.M., Schultz, N., Lundback, T., Einarsdottir, B.O., Saleh, A., Gokturk, C., Baranczewski, P., Svensson, R., Berntsson, R.P., Gustafsson, R., Stromberg, K., Sanjiv, K., Jacques-Cordonnier, M.C., Desroses, M., Gustavsson, A.L., Olofsson, R., Johansson, F., Homan, E.J., Loseva, O., Brautigam, L., Johansson, L., Hoglund, A., Hagenkort, A., Pham, T., Altun, M., Gaugaz, F.Z., Vikingsson, S., Evers, B., Henriksson, M., Vallin, K.S., Wallner, O.A., Hammarstrom, L.G., Wiita, E., Almlof, I., Kalderen, C., Axelsson, H., Djureinovic, T., Puigvert, J.C., Haggblad, M., Jeppsson, F., Martens, U., Lundin, C., Lundgren, B., Granelli, I., Jensen, A.J., Artursson, P., Nilsson, J.A., Stenmark, P., Scobie, M., Berglund, U.W. and Helleday, T. (2014) MTH1 inhibition eradicates cancer by preventing sanitation of the dNTP pool. Nature 508, 215–221.
[19] Huber, K.V., Salah, E., Radic, B., Gridling, M., Elkins, J.M., Stukalov, A., Jemth, A.S., Gokturk, C., Sanjiv, K., Stromberg, K., Pham, T., Berglund, U.W., Colinge, J., Bennett, K.L., Loizou, J.I., Helleday, T., Knapp, S. and Superti-Furga, G. (2014) Stereospecific targeting of MTH1 by (S)-crizotinib as an anticancer strategy. Nature 508, 222–227.
[20] Smalås, A.O., Leiros, H.K., Os, V. and Willassen, N.P. (2000) Cold adapted enzymes. Biotechnol. Annu. Rev. 6, 1–57.
[21] Lonhienne, T., Gerday, C. and Feller, G. (2000) Psychrophilic enzymes: revisiting the thermodynamic parameters of activation may explain local flexibility. Biochim. Biophys. Acta 1543, 1–10.
[22] Svensson, L.M., Jemth, A.S., Desroses, M., Loseva, O., Helleday, T., Hogbom, M. and Stenmark, P. (2011) Crystal structure of human MTH1 and the 8-oxo-dGMP product complex. FEBS Lett. 585, 2617–2621.
[23] Baykov, A.A., Evtushenko, O.A. and Avaeva, S.M. (1988) A malachite green procedure for orthophosphate determination and its use in alkaline phosphatase-based enzyme immunoassay. Anal. Biochem. 171, 266–270.
[24] Kabsch, W. (2010) XDS. Acta Crystallogr. D Biol. Crystallogr. 66, 125–132.
[25] Collaborative Computational Project, N (1994) The CCP4 suite: programs for protein crystallography. Acta Crystallogr. D Biol. Crystallogr. 50, 760–763.
[26] McCoy, A.J., Grosse-Kunstleve, R.W., Adams, P.D., Winn, M.D., Storoni, L.C. and Read, R.J. (2007) Phaser crystallographic software. J. Appl. Crystallogr. 40, 658–674.
[27] Emsley, P. and Cowtan, K. (2004) Coot: model-building tools for molecular graphics. Acta Crystallogr. D Biol. Crystallogr. 60, 2126–2132.
[28] Biasini, M., Bienert, S., Waterhouse, A., Arnold, K., Studer, G., Schmidt, T., Kiefer, F., Cassarino, T.G., Bertoni, M., Bordoli, L. and Schwede, T. (2014) SWISS-MODEL: modelling protein tertiary and quaternary structure using evolutionary information. Nucleic Acids Res. 42 (w1), w252–w258.
[29] McDonald, I.K. and Thornton, J.M. (1994) Satisfying hydrogen bonding potential in proteins. J. Mol. Biol. 238, 777–793.
[30] Vriend, G. (1990) WHAT IF: a molecular modeling and drug design program. J. Mol. Graph. 8 (52–6), 29.
[31] Gerday, C. (2013) Psychrophily and catalysis. Biology 2, 719–741.
[32] Bjelic, S., Brandsdal, B.O. and Aqvist, J. (2008) Cold adaptation of enzyme reaction rates. Biochemistry 47, 10049–10057.
[33] Feller, G. and Gerday, C. (2003) Psychrophilic enzymes: hot topics in cold adaptation. Nat. Rev. Microbiol. 1, 200–208.
[34] Huang, H.L., Su, H.T., Wu, C.H. and Tsai-Wu, J.J. (2014) A molecular biological and biochemical investigation on *mycobacterium tuberculosis* MutT protein. Jundishapur J. Microbiol. 7, e9367.
[35] Saraswat, V., Azurmendi, H.F. and Mildvan, A.S. (2004) Mutational, NMR, and NH exchange studies of the tight and selective binding of 8-oxo-dGMP by the MutT pyrophosphohydrolase. Biochemistry 43, 3404–3414.
[36] Lanes, O., Leiros, I., Smalas, A.O. and Willassen, N.P. (2002) Identification, cloning, and expression of uracil-DNA glycosylase from Atlantic cod (*Gadus morhua*): characterization and homology modeling of the cold-active catalytic domain. Extremophiles 6, 73–86.
[37] Raeder, I.L., Leiros, I., Willassen, N.P., Smalås, A.O. and Moe, E. (2008) Uracil-DNA N-glycosylase (UNG) from the marine, psychrophilic bacterium *Vibrio salmonicida* shows cold adapted features. A comparative analysis to *Vibrio cholerae* uracil-DNA N-glycosylase. Enzyme Microb. Technol. 42, 594–600.
[38] Outzen, H., Berglund, G.I., Smalås, A.O. and Willassen, N.P. (1996) Temperature and pH sensitivity of trypsins from Atlantic salmon (*Salmo salar*) in comparison with bovine and porcine trypsin. Comp. Biochem. Physiol. B: Biochem. Mol. Biol. 115, 33–45.
[39] Schroder Leiros, H.K., Willassen, N.P. and Smalås, A.O. (2000) Structural comparison of psychrophilic and mesophilic trypsins. Elucidating the molecular basis of cold-adaptation. Eur. J. Biochem. 267, 1039–1049.
[40] Feller, G. (2013) Psychrophilic enzymes: from folding to function and biotechnology. Scientifica 2013, 512840.
[41] Siddiqui, K.S. and Cavicchioli, R. (2006) Cold-adapted enzymes. Annu. Rev. Biochem. 75, 403–433.
[42] Isaksen, G.V., Åqvist, J. and Brandsdal, B.O. (2014) Protein surface softness is the origin of enzyme cold-adaptation of trypsin. PLoS Comput. Biol. 10, e1003813.
[43] Fedøy, A.E., Yang, N., Martinez, A., Leiros, H.K. and Steen, I.H. (2007) Structural and functional properties of isocitrate dehydrogenase from the psychrophilic bacterium *Desulfotalea psychrophila* reveal a cold-active enzyme with an unusual high thermal stability. J. Mol. Biol. 372, 130–149.
[44] Leiros, H.K., Willassen, N.P. and Smalås, A.O. (1999) Residue determinants and sequence analysis of cold-adapted trypsins. Extremophiles 3, 205–219.
[45] Galperin, M.Y., Moroz, O.V., Wilson, K.S. and Murzin, A.G. (2006) House cleaning, a part of good housekeeping. Mol. Microbiol. 59, 5–19.